Applied Physics Letters ARTICLE pubs.aip.org/aip/apl

Detection of spin current generated by the acoustic spin–rotation coupling mechanism via acoustic voltage

Cite as: Appl. Phys. Lett. **125**, 252402 (2024); doi: 10.1063/5.0242879
Submitted: 8 October 2024 · Accepted: 5 December 2024 ·
Published Online: 16 December 2024

Shuai Mi, Chenbo Zhao, Meihong Liu, Jianbo Wang, and Qingfang Liu[a]

AFFILIATIONS

School of Physical Science and Technology, Lanzhou University, Lanzhou 730000, People's Republic of China

[a]Author to whom correspondence should be addressed: liuqf@lzu.edu.cn

ABSTRACT

The method of combining surface acoustic waves (SAWs) with electrical detection has promoted the study of phonon–spin coupling and spintronics. Aiming at problems of difficult detection of DC voltage and unknown origin of spin current caused by SAW in ferromagnetic/light metal systems, we constructed the Ni/Cu/Ta on $LiNbO_3$ substrate and measured acoustic voltages directly, which are used to analyze the spin current induced by SAW. By analyzing the angular dependence of acoustic voltages and estimating the maximum spin current, it is determined that acoustic voltages originate from the acoustic spin–rotation (ASR) coupling and the acoustic spin pumping (ASP) effects. The angular dependence shows that for the longitudinal voltage, the contribution of ASR to ASP is in the ratio of 3.22/3.77, while the transverse voltage is mainly contributed by the ASR. The maximum spin current due to ASR is 0.97×10^5 A/m^2, while that due to ASP is 1.47×10^5 A/m^2. This work provides ideas for the design of phonon–spin coupled devices.

The application of acoustic waves, including surface acoustic waves (SAWs)[1] and bulk acoustic wave, to spintronic devices has significantly advanced the field of spintronics, leading to the emergence of a new subfield known as acoustic spintronics.[2] Similar to conventional spintronics, acoustic spintronics involves the manipulation of electron spins using phonons or acoustic waves, with the aim of further manipulating the state of magnetization[3] to create energy-efficient, nonvolatile memories and logic devices. Following metal spintronics and semiconductor spintronics, it has gradually become a new research topic[4,5] in the spintronics field in recent years. The SAW, a kind of mechanical wave that propagates on the surface of the solid, causes periodic strains on the surface of the substrate, which in turn causes the precession of magnetic moments[6] in a magnetic film on the substrate. This is usually achieved by magneto-elastic coupling effect,[7] magnetoelectric coupling effect,[8] or spin–rotation coupling effect.[9] In the bilayer film structure consisting of the ferromagnetic layer and a nonmagnetic layer (FM/NM bilayer), the spin current can be generated by these effects, and then the spin current is converted into the charging current by the inverse spin Hall effect (ISHE), and finally a direct-current (DC) voltage can be detected.

A classical study has demonstrated that the DC voltage could be generated by the acoustic spin pumping effect[10] in the Co/Pt bilayer structure. This effect is typically accompanied by the magnetization precession or ferromagnetic resonance,[11] where the SAW pumps out the spin current from the ferromagnetic material to the nonmagnetic material. A combination of longitudinal and transverse DC voltage detection in Ni/Cu(Ag)/Bi_2O_3 induced by the Rayleigh-type SAW indicates that the spin current can be converted into to the charge current through the magnon–phonon coupling and the inverse Edelstein effect.[12] It has been reported that the anomalous Nernst effect[13] caused by SAW could also lead to the charge accumulation in $[Co/Pd]_3$, generating a measurable DC voltage. Moreover, the acoustic spin Hall effect[14] in X/CoFeB/MgO (X = Pt, W, and Cu) and the unidirectional planar Hall effect[15] in CoFeB/Ta/MgO, induced by SAW, manifest themselves as a field-dependent acoustic voltage. In the presence of SAWs, the DC voltage in the Ni strip sample exhibits behavior characteristic of an anisotropic magnetoresistance (AMR) rectification[16] voltage signal. The spin–rotation coupling effect[17] due to SAW can also cause a spin current, which can be injected into the magnetic layer[18] to drive a ferromagnetic resonance. However, the DC voltage due to SAW is rarely reported in the FM/NM structure, where the NM layer is a weak spin–orbit interaction (SOI) material. The generation mechanism of the spin current or DC voltage in them is also unclear.

In this work, we investigate acoustic voltages in Ni/Cu/Ta film. Through the measurement of the angular dependence of acoustic

voltage and estimation of the maximum spin current, we have ascertained that the acoustic voltage originates mainly from the acoustic spin–rotation (ASR) coupling effect and the acoustic spin pumping (ASP) effect. The result on angular dependence reveals that the contribution ratio of ASR to ASP for the longitudinal voltage is about 3.22/3.77, while the transverse voltage is mainly contributed by the ASR. Our calculation results show that the maximum spin current caused by the ASR and ASP in the Ni/Cu/Ta is of the same order of magnitude (10^5 A/m^2). The detection and analysis of acoustic voltage provide a powerful experimental verification for the phonon–spin coupling. Moreover, it is helpful to design novel electrical devices and to advance the development of acoustic spin electronics.

Ta(3 nm)/Ni(20 nm)/Cu(5 nm)/Ta(3 nm) is prepared on a 128°-Y cut $LiNbO_3$ substrate, and the interdigital transducers (IDTs) structure is sub./Ta(3 nm)/Au(40 nm), as shown in Fig. 1(a). The SAW propagates along the x axis and the external magnetic field is at an angle θ to the positive direction of the x axis. The voltage signals, including longitudinal voltage (V_{xx}) and transverse voltage (V_{xy}), are measured in the x axis and y axis. The optical image of the SAW device (Fig. S1) and the detailed voltage measurement method are presented in supplementary material S1. Figure 1(b) shows the parameters S_{11} and S_{12} of the SAW device, which indicates that the IDTs could excite the SAW with the first of 160 MHz, and the fifth of 789 MHz. Under the fifth SAW, the acoustic voltage changes (ΔV_{xx} and ΔV_{xy}) in the x axis and y axis exhibit different shapes and amplitudes at the same magnetic field angle, as shown in Figs. 1(c) and 1(d). ΔV_{xx} (ΔV_{xy}) is calculated by $\Delta V_{xx} = V_{xx} - V_{Ms}$ ($\Delta V_{xy} = V_{xy} - V_{Ms}$), where V_{xx} (ΔV_{xy}) and V_{Ms} are the value of the acoustic voltage measured at a certain external magnetic field and the saturated external magnetic field, respectively. When the SAW travels with $+k$ (IDT1), a relatively large voltage peak appears at positive H for ΔV_{xx}, and when the SAW travels with $-k$ (IDT2), a relatively strong voltage peak appears at negative H. This demonstrates that the acoustic voltages are nonreciprocal, which is similar to the nonreciprocity observed in the SAW transmission spectrum.[19]

Figures 2(a) and 2(b) show the acoustic voltage V_{xx} and V_{xy} as functions of the external magnetic field for the Ni/Cu/Ta film, respectively. The angle θ is 45°, 135°, 180°, 225°, and 315°. It exhibits the downward voltage peak in range of positive or negative magnetic field. For the V_{xx} shown in Fig. 2(a), within the range of positive or negative magnetic fields, the linear shape of the voltage signal displays a similar Lorentz-symmetric linear shape. A distinctive feature of the voltage signal in the Ni/Cu/Ta film is that the peak shape remains downward when the magnetic field is reversed. This result for Ni/Cu/Ta is different from that for Ni/Pt[20] or Ni/Cu/Bi_2O_3,[21] as the latter two exhibit an upward and downward peak in the positive and negative magnetic field, respectively. For the V_{xy} shown in Fig. 2(b), the acoustic voltage line's shape is slightly different from that of V_{xx}. Although the voltage lines are still dominated by Lorentzian symmetry lines, there exist small peaks near zero field at a few special angles, like 135° and 315°.

The complete acoustic voltage variations (ΔV_{xx} and ΔV_{xy}) with the external magnetic field angle are shown in Figs. 2(c) and 2(d). The external magnetic field is swept with θ increasing from 0° to 360° in steps of 5°. The use of ΔV instead of V here is intended to preserve only the characteristics of the acoustic voltage shape in the mapping plots while removing the impact of differences in voltage values at different magnetic field angles on the mapping plots. For ΔV_{xx}, in the range of 0°–180° or 180°–360°, the change of the voltage signal is based on a period of 90°. ΔV_{xx} in Fig. 2(c) also shows nonreciprocity of the acoustic voltage, which depends on the angle of the external magnetic field. For ΔV_{xy}, the period of the voltage signal changes with a period of approximately 180°. This difference indicates that the mechanism of voltage generation by SAW may be different in the x axis direction and in the y axis direction.

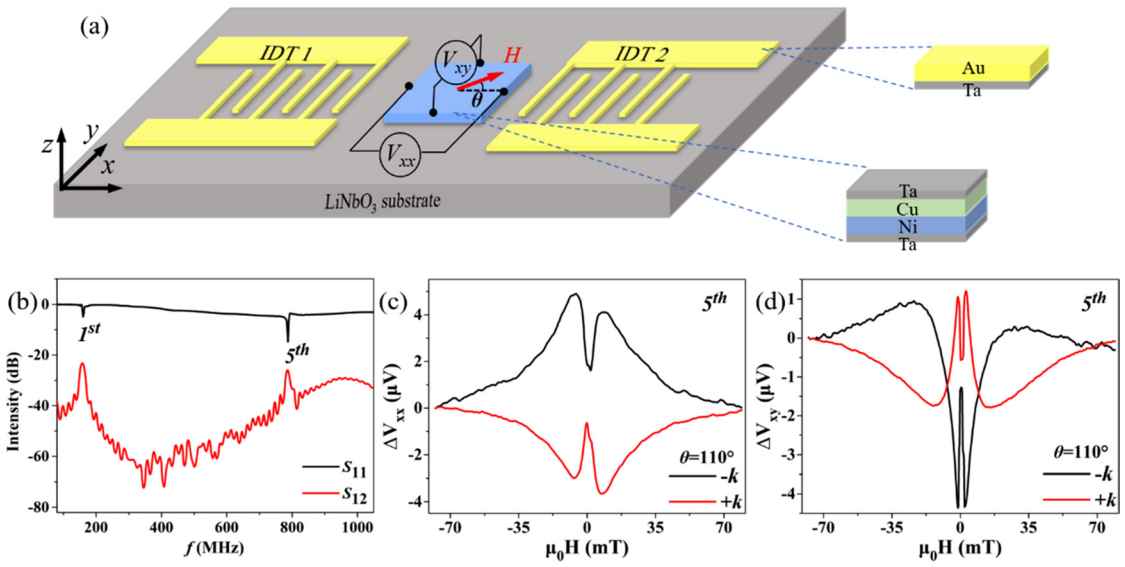

FIG. 1. Experimental setup and DC acoustic voltage measurements in the SAW device. (a) Schematic illustration of the experimental setup. The acoustic voltages (V_{xx} and V_{xy}) are measured when the SAW and the in-plane magnetic field (H) at an angle of θ act together on a magnetic film. (b) The *S* parameter of the SAW device. (c) and (d) The acoustic voltage changes (ΔV_{xx} and ΔV_{xy}) for $+k$ and $-k$ at $\theta = 110°$.

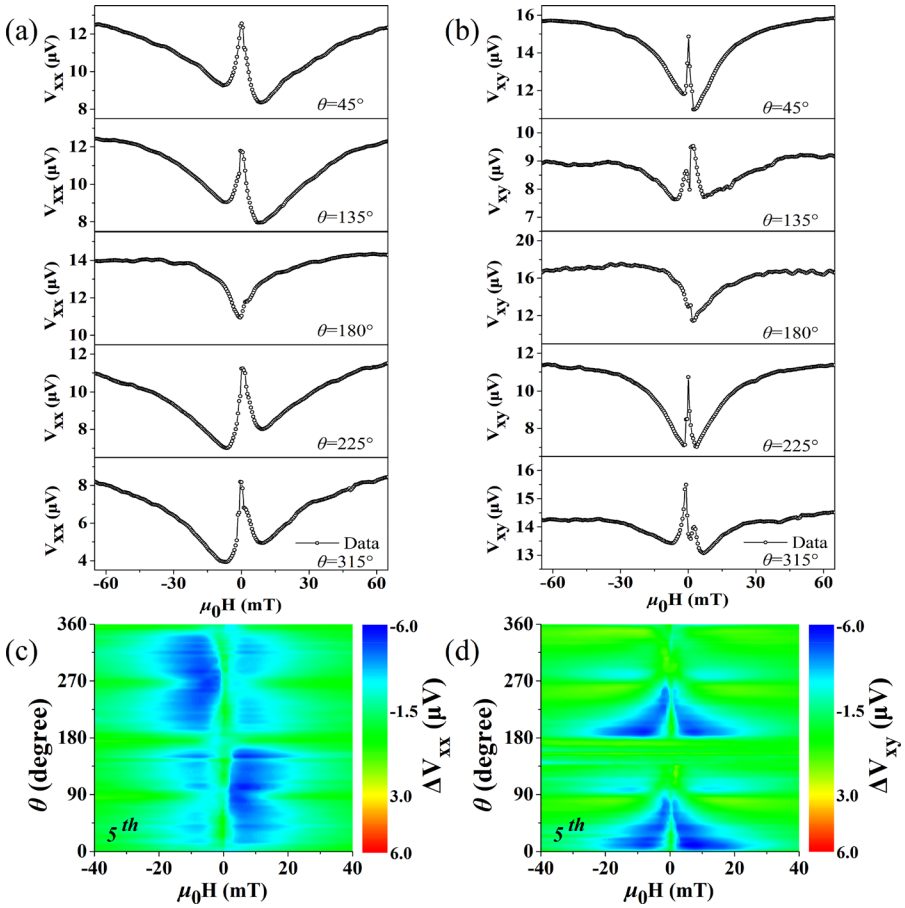

FIG. 2. Acoustic voltages at different external magnetic field angles. (a) and (b) The magnetic field dependence of the acoustic voltage (V_{xx} and V_{xy}) at different angles. (c) and (d) The mapping of ΔV_{xx} and ΔV_{xy} dependence of the external magnetic field angle.

The voltages in Figs. 2(a) and 2(b) show that the sign of acoustic voltages does not change as the external magnetic field reverses its direction. So, it seems that the ASP is not the main cause of acoustic voltage in our film, since the most obvious feature for the ASP is that there is a sign reversal of the peak with the reversal of H direction.[10,22] However, due to the existence of Ta (having spin–orbit coupling) and larger spin diffusion length of Cu,[23] spin pumping effect may also contribute to acoustic voltages. FMR based on magnetoelastic coupling is not the main cause of acoustic voltage in our film either since FMR shows positive and negative voltage peaks with change of the magnetic field angle.[16,24] In addition to the magnetoelastic coupling effect, the spin in the film and the mechanical rotation in lattice could be directly coupled, which is known as spin–vorticity coupling[25] or spin–rotation coupling (SRC). Previous reports[17] have shown that materials with weak spin orbitals, such as Cu, are favorable for the generation of spin currents based on spin–rotation coupling. The spin current generated by spin–rotation coupling has been verified in $Ni_{81}Fe_{19}$/Cu samples.[18] So, the spin–rotation coupling may play an important role in the generation of spin current or acoustic voltage in this case of microelectromechanical systems.

In order to analyze the mechanism of acoustic voltage in our sample, considering the imperfect Lorenz-symmetric linear shape of our measuring results, we suppose the acoustic voltage spectrum is decomposed into symmetric (V_s) and antisymmetric (V_a) components.[16] Considering the influence of RF magnetic fields, we write the acoustic voltage as

$$V_{SAW} = V_{s1}\frac{(\Delta H_1)^2}{(H-H_{r1})^2+(\Delta H_1)^2} + V_{a1}\frac{\Delta H_1(H-H_{r1})}{(H-H_{r1})^2+(\Delta H_1)^2} + V_{s2}\frac{(\Delta H_2)^2}{(H-H_{r2})^2+(\Delta H_2)^2} + V_{a2}\frac{\Delta H_2(H-H_{r2})}{(H-H_{r2})^2+(\Delta H_2)^2}. \quad (1)$$

Here, H is the external magnetic field, V_{s1}, V_{a1}, H_{r1}, and ΔH_1 are the symmetric component, the antisymmetric component, the oscillation field, and the oscillation linewidth for the main oscillation peak, respectively. V_{s2}, V_{a2}, H_{r2}, and ΔH_2 are the symmetric component, the antisymmetric component, the oscillation field, and the oscillation linewidth for the secondary oscillation peak, such as when $\theta = 135°$ in Fig. 2(b), respectively. In this work, the oscillation peak near the zero magnetic field is caused by the RF magnetic field generated by the RF current in the IDTs (see supplementary material S2 for detailed evidence) and is not a major factor to consider when analyzing the DC voltage caused by SAW.

In the positive magnetic field range, the acoustic voltage curves are fitted using Eq. (1) at each magnetic angle θ to obtain the symmetric and antisymmetric components of the acoustic voltage. Figure 3(a)

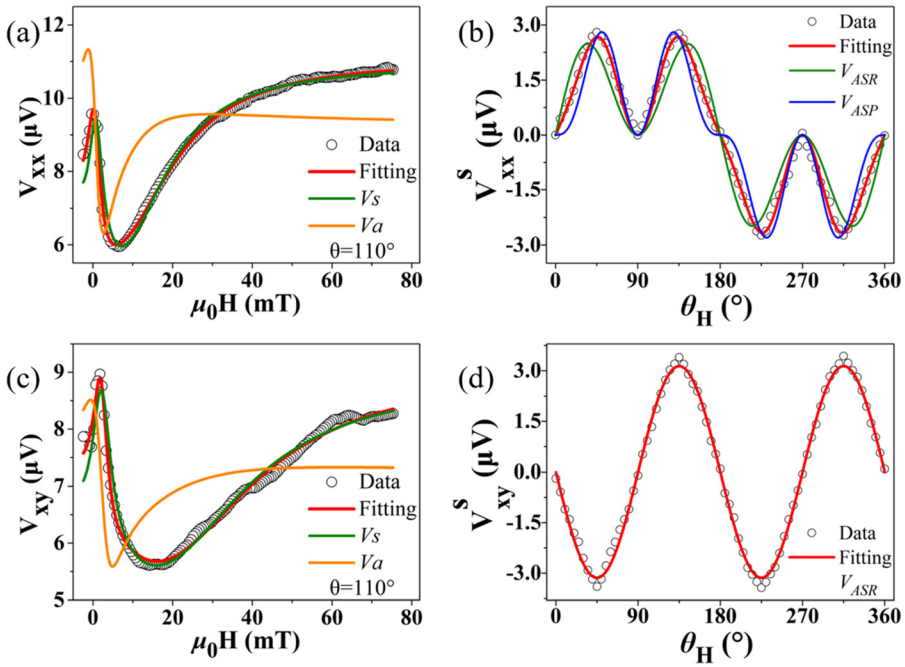

FIG. 3. (a) and (c) The acoustic voltage V_{xx} and V_{xy} are divided into symmetric (V_s) and antisymmetric (V_a) signals at $\theta = 110°$. (b) The angle dependence of the V_s for V_{xx}. The red line is fitted according to Eq. (2). The green and blue lines represent the contribution by ASR coupling (V_{ASR}) and ASP effect (V_{ASP}), respectively. (d) The angle dependence of V_s for V_{xy}. The red line is fitted by Eq. (3) and contributed by V_{ASR}.

shows the fitting result of V_{xx} at θ of 110°. The green and orange lines are the fitting results of V_s (V_{s1}) and V_a (V_{a1}), respectively. Similar to the method reported by Chen *et al.*,[16] who used V_s to analyze the voltage spectrum in studying SAW-induced FMR, we analyze V_s spectra as a function of θ to investigate the mechanism of acoustic voltage. Based on the above results, we suppose both ASR and ASP contribute to the acoustic voltage.

For V_{xx}, by fitting the relationship between the V_s and the angle of external magnetic field, we directly get the angular dependence of V_s, which is summarized in the following expression:

$$V_S = V_{ASR} \sin 2\theta \cos\theta + V_{ASP} \sin^2 2\theta \sin\theta. \quad (2)$$

For V_{xy}, by fitting the relationship between V_s and the angle of external magnetic field, the angular dependence of V_s shows a different expression, as follows:

$$V_S = V_{ASR} \sin 2\theta, \quad (3)$$

where θ is the angle between the external magnetic field and the positive direction of the x axis. V_{ASR} and V_{ASP} are considered to be the voltage signals contributed by the ASR coupling and ASP effects, respectively. The ASR voltage signal exhibits a $\sin 2\theta$ angular dependence, and the projection of the V_{ASR} along the x axis shows the contribution $\cos\theta$. The ASP shows a $\sin^2 2\theta$ angular dependence, and the projection of V_{ASP} along the x axis shows a residual contribution as the $\sin\theta$.

Figure 3(b) shows the relationship between V_s and the angle of external magnetic field, where V_s is fitted by using Eq. (2). The green line is the fitting result considering only the V_{ASR} term in Eq. (2), and the blue line is the fitting result considering only the V_{ASP} term. In the fitting, we find that ASR and ASP jointly contribute to the acoustic voltage in the x axis direction, and the fitting coefficients show that the contribution ratio is about 3.22/3.77.

For the acoustic voltage on the y axis (V_{xy}), Fig. 3(c) shows the fitting result of V_{xy} at a θ of 110° in the positive magnetic field range. Identical to the results of V_{xx}, V_s plays a dominant role. Figure 3(d) shows the relationship between V_s and the angle of external magnetic field, which is different from Fig. 3(b). By fitting V_s [according to Eq. (3)], it is easily seen that the acoustic voltage in the y axis direction is mainly contributed by the ASR.

The perfect fitting of our experimental data indicates that both ASR coupling and ASP contribute to the acoustic voltage in our sample. Figure 4 shows an illustration of ASR coupling and ASP in our Ni/Cu/Ta film. As shown in Fig. 4(a), when the external magnetic field and the SAW are applied in the direction of x axis, the spin direction $\boldsymbol{\sigma}$ is in the direction of the vector sum of spin $\boldsymbol{\sigma}_{\mathbf{H}}$ (the spin vector due to applied field) and spin $\boldsymbol{\sigma}_{\mathbf{SAW}}$ (the spin vector due to the rotational transfer of SAW's phonon angular momentum[26]). For a Rayleigh-type SAW, the angular velocity gradient of the macroscopic rotation[20] in the thickness direction could cause a gradient of spin accumulation. As shown in Fig. 4(a), the pure spin current ($\mathbf{J}_s'$) generated in the Cu layer is injected into the FM layer. As a result, a spin transfer torque is exerted on the magnetization and an FMR is excited in the FM layer.[18] The FMR can also be excited based on magneto-elastic coupling. The FMR generates a spin current ($\mathbf{J}_s$), which is injected back into the Cu layer and Ta layer due to the ASP, where the spin current is converted into a charge current by ISHE in Ta. Finally, a DC voltage is detected.

Some studies[20,27] have demonstrated that in the presence of a SAW, there is an angle between the directions of the magnetic moment (or the direction of the spin injected into the magnetic layer) and the external magnetic field. The spin $\boldsymbol{\sigma}$ can always be decomposed into two spins in mutually perpendicular directions, such as spin $\boldsymbol{\sigma}_x'$ in the x axis and spin $\boldsymbol{\sigma}_y'$ in the y axis direction. Correspondingly, the DC voltage due to the ISHE detected in the Ta layer can also be decomposed into the voltage V_{xx} in the x axis and the voltage V_{xy} in the

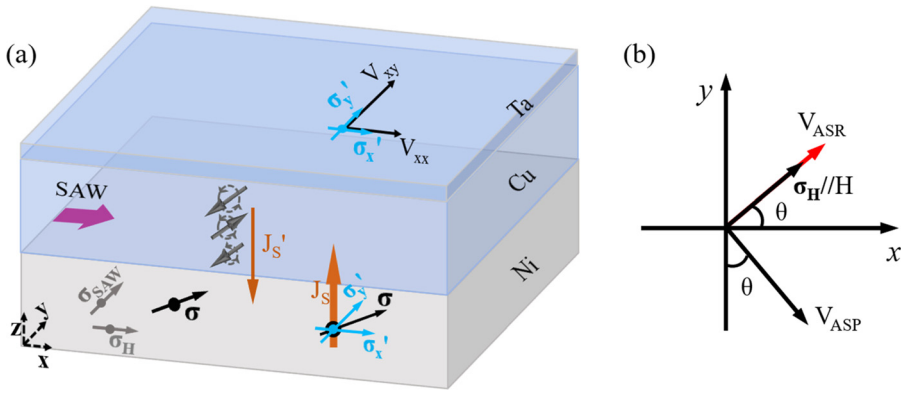

FIG. 4. (a) Illustration of the ASR coupling and ASP in the Ni/Cu/Ta film. The spin $\boldsymbol{\sigma}_{SAW}$ (y axis) due to the SAW is perpendicular to the SAW propagation direction (x axis). The spin $\boldsymbol{\sigma}_{SAW}$ couples to the electron spins and then the spin current $\mathbf{J}_s'$, caused by the gradient of mechanical rotation, flows in the z axis direction. The spin $\boldsymbol{\sigma}_H$ due to the external magnetic field is along the x axis, and the actual spin $\boldsymbol{\sigma}$ is in the direction of the vector sum of $\boldsymbol{\sigma}_H$ and $\boldsymbol{\sigma}_{SAW}$. The spin $\boldsymbol{\sigma}$ can always be decomposed into two spins in mutually perpendicular directions, such as spin $\boldsymbol{\sigma}_x'$ in the x axis and spin $\boldsymbol{\sigma}_y'$ in the y axis direction. The spin $\boldsymbol{\sigma}$ pumps a spin current $\mathbf{J}_s$ into the Cu and Ta layer under the action of SAW. $\mathbf{J}_s$ is converted into the charge current by the ISHE and the DC voltage can be detected in the two directions (V_{xx} and V_{xy}). (b) Schematic diagram of $\boldsymbol{\sigma}_H$, V_{ASR}, and V_{ASP}. V_{ASR} generated by the ASR exhibits a voltage along the direction of the magnetic field H.

y axis directions. It is worth mentioning that the voltage caused by ASP is always in the direction perpendicular to the direction of $\boldsymbol{\sigma}_H$. Typically, the voltage in the direction perpendicular to the external magnetic field (H) is considered to be the voltage V_{ASP}. In this case, the voltage in the direction perpendicular to V_{ASP} is considered as V_{ASR}. V_{ASR} and V_{ASP} and their projection relationship in x axis or y axis are shown in Fig. 4(b).

Finally, we estimate the magnitude of the spin current generated by ASR in the sample. The method reported in Refs. 9, 17, and 18 was used to calculate the spin current generated by the ASR. If $\omega\tau_{sf} \ll 1$ and $\lambda_s k_t \ll 1$, the y-polarized spin current can be expressed as[17]

$$J_s \approx \omega\tau_{sf}\frac{\hbar\sigma_0}{2e}\frac{\omega^3 u_0}{c_t^2}\frac{\sqrt{1-\xi^2}}{\xi}e^{-k_t z+i(kx-\omega t+\pi/2)}. \quad (4)$$

Here, ω, c_t, and u_0 are the angle frequency, velocity, and amplitude of the mechanical rotation caused by the SAW, respectively. τ_{sf}, $\hbar$, σ_0, and λ_s are the spin lifetime, Planck's constant, conductivity, and spin diffusion length, respectively. e is the electric charge. ξ is a constant given by $\xi \approx (0.875 + 1.12\nu)/(1+\nu)$ with ν being Poisson's ratio.[18] k and k_t are the wave number and transverse wave number of the SAW. k is given by $\omega = c_t k\xi$, and k_t is given by $k_t = k\sqrt{1-\xi^2}$. z is the distance from the film surface along the thickness direction.

In this case, $\omega/2\pi = f = 789$ MHz, the amplitude of mechanical rotation u_0 is estimated as 1 nm.[17] When z is considered as 0 (at the maximum mechanical rotation) and the phase is not considered, the spin current could be estimated. The values of τ_{sf}, σ_0, c_t, and ν for Cu reported by Mamoru Matsuo[17] are used. The maximum amplitude of spin current due to ASR is about $0.970\,45 \times 10^5$ A/m^2. The spin current generated by ASP is estimated in supplementary material S3. The spin current due to the ASP is about $1.472\,58 \times 10^5$ A/m^2.

In summary, we have demonstrated that the acoustic voltage induced by SAW originates from the acoustic spin–rotation coupling effect and the acoustic spin pumping effect by analyzing the angular dependence of the acoustic voltage and calculating the maximum spin current. The directly measured acoustic voltages are used to analyze the spin current induced by the SAW. The angular dependence of the acoustic voltage shows that the contribution of ASR and ASP to the x axis acoustic voltage is in the ratio of 3.22/3.77, while the y axis acoustic voltage is mainly contributed by the ASR. The maximum amplitude of the spin current due to the ASR is calculated to be about $0.970\,45 \times 10^5$ A/m^2, while that due to the ASP is about $1.472\,58 \times 10^5$ A/m^2. The maximum spin current caused by the ASR or ASP in Ni/Cu/Ta is of the same order of magnitude. In a ferromagnetic/light metal (Cu)/Ta structure, the acoustic spin–rotation coupling effect plays a major role in the generation of spin currents or acoustic voltages. We obtained the acoustic voltage using a weak SOI material Cu and verified its generation mechanism. This provides powerful experimental verification and experimental ideas for the application of SAWs to generate spin currents, drive magnetization precession, etc.

See the supplementary material for details on the SAW device (S1), the influence of microwave magnetic field (S2), and the spin current due to ASP (S3) and for a discussion of the nonlinear effects (S4).

This work is supported by the National Natural Science Foundation of China (Nos. 12074158, 12174166, and 12304144) and the Fundamental Research Funds for the Central Universities (lzujbky-2024-22).

AUTHOR DECLARATIONS

Conflict of Interest

The authors have no conflicts to disclose.

Author Contributions

Shuai Mi: Conceptualization (equal); Data curation (equal); Investigation (equal); Methodology (equal); Writing – original draft (equal); Writing – review & editing (equal). **Chenbo Zhao:** Data curation (equal); Funding acquisition (equal); Methodology (equal). **Meihong Liu:** Formal analysis (equal); Methodology (equal). **Jianbo Wang:** Conceptualization (equal); Funding acquisition (equal);

Resources (equal); Writing – review & editing (equal). **Qingfang Liu:** Conceptualization (equal); Funding acquisition (equal); Methodology (equal); Project administration (equal); Supervision (equal); Writing – review & editing (equal).

DATA AVAILABILITY

The data that support the findings of this study are available from the corresponding author upon reasonable request.

REFERENCES

[1]L. Dreher, M. Weiler, M. Pernpeintner, H. Huebl, R. Gross, M. S. Brandt, and S. T. B. Goennenwein, Phys. Rev. B **86**, 134415 (2012).
[2]K. Uchida, H. Adachi, T. An, T. Ota, M. Toda, B. Hillebrands, S. Maekawa, and E. Saitoh, Nat. Mater. **10**, 737 (2011).
[3]J. Puebla, Y. Hwang, S. Maekawa, and Y. Otani, Appl. Phys. Lett. **120**, 220502 (2022).
[4]W.-G. Yang and H. Schmidt, Appl. Phys. Rev. **8**, 021304 (2021).
[5]Y. Yang, L. Zhao, D. Yi, T. Xu, Y. Chai, C. Zhang, D. Jiang, Y. Ji, D. Hou, W. Jiang, J. Tang, P. Yu, H. Wu, and T. Nan, Nat. Commun. **15**, 1018 (2024).
[6]M. Weiler, L. Dreher, C. Heeg, H. Huebl, R. Gross, M. S. Brandt, and S. T. B. Goennenwein, Phys. Rev. Lett. **106**, 117601 (2011).
[7]T. Funato and M. Matsuo, Phys. Rev. Lett. **128**, 077201 (2022).
[8]Y. Ba, S. Zhuang, Y. Zhang, Y. Wang, Y. Gao, H. Zhou, M. Chen, W. Sun, Q. Liu, G. Chai, J. Ma, Y. Zhang, H. Tian, H. Du, W. Jiang, C. Nan, J. M. Hu, and Y. Zhao, Nat. Commun. **12**, 322 (2021).
[9]J. Ieda, M. Matsuo, and S. Maekawa, Solid State Commun. **198**, 52 (2014).
[10]M. Weiler, H. Huebl, F. S. Goerg, F. D. Czeschka, R. Gross, and S. T. Goennenwein, Phys. Rev. Lett. **108**, 176601 (2012).
[11]Y. Hwang, J. Puebla, K. Kondou, and Y. Otani, Adv. Mater. Interfaces **9**, 2201432 (2022).
[12]M. Xu, J. Puebla, F. Auvray, B. Rana, K. Kondou, and Y. Otani, Phys. Rev. B **97**, 180301(R) (2018).
[13]C. Chen, S. Fu, L. Han, R. Su, P. Liu, R. Chen, W. Zhu, L. Liao, F. Pan, and C. Song, Adv. Electron. Mater. **8**, 2200593 (2022).
[14]T. Kawada, M. Kawaguchi, T. Funato, H. Kohno, and M. Hayashi, Sci. Adv. **7**, eabd9697 (2021).
[15]T. Kawada, M. Kawaguchi, and M. Hayashi, Phys. Rev. B **99**, 184435 (2019).
[16]C. Chen, L. Han, P. Liu, Y. Zhang, S. Liang, Y. Zhou, W. Zhu, S. Fu, F. Pan, and C. Song, Adv. Mater. **35**, 2302454 (2023).
[17]M. Matsuo, J. Ieda, K. Harii, E. Saitoh, and S. Maekawa, Phys. Rev. B **87**, 180402(R) (2013).
[18]D. Kobayashi, T. Yoshikawa, M. Matsuo, R. Iguchi, S. Maekawa, E. Saitoh, and Y. Nozaki, Phys. Rev. Lett. **119**, 077202 (2017).
[19]R. Sasaki, Y. Nii, Y. Iguchi, and Y. Onose, Phys. Rev. B **95**, 020407(R) (2017).
[20]Y. Cao, H. Ding, Y. Zuo, X. Li, Y. Zhao, T. Li, N. Lei, J. Cao, M. Si, L. Xi, C. Jia, D. Xue, and D. Yang, Nat. Commun. **15**, 1013 (2024).
[21]J. Puebla, M. Xu, B. Rana, K. Yamamoto, S. Maekawa, and Y. Otani, J. Phys. D **53**, 264002 (2020).
[22]K. Ando, S. Takahashi, J. Ieda, Y. Kajiwara, H. Nakayama, T. Yoshino, K. Harii, Y. Fujikawa, M. Matsuo, S. Maekawa, and E. Saitoh, J. Appl. Phys. **109**, 103913 (2011).
[23]H. Wang, C. Du, P. Chris Hammel, and F. Yang, Appl. Phys. Lett. **104**, 202405 (2014).
[24]R. Gao, Y. Ye, H. Wu, X. Li, X. Liu, J. Wang, and Q. Liu, Appl. Phys. Lett. **121**, 042401 (2022).
[25]Y. Kurimune, M. Matsuo, and Y. Nozaki, Phys. Rev. Lett. **124**, 217205 (2020).
[26]R. Sasaki, Y. Nii, and Y. Onose, Nat. Commun. **12**, 2599 (2021).
[27]S. Davis, A. Baruth, and S. Adenwalla, Appl. Phys. Lett. **97**, 232507 (2010).